A study of the efficient approach to introduce two Na ions into a $NaVOPO_4$ matrix and an analysis of the electrochemical performance of $NaVOPO_4/Na_2V(PO_4)_2$

A. Neelaveni, N. Sivakumar*
PG and Research Department of Physics, Chikkaiah Naicker College, Erode– 638004, Tamilnadu, India

In this work, we manufacture NaVOPO4 with the addition of one additional Na ion to enhance the stability and electrochemical formulation utilizing three ways, including sol gel-assisted hydrothermal, pure sol-gel, and solid state reaction methods. The sol-gel aided hydrothermal approach is the most effective way to add more Na ions to the $NaVOPO_4$ matrix out of the three. Due to the presence of carbon content in high temperatures, the alterations of oxygen environment (O (1 &2) sites around the Na and V cause $NaVOPO_4$/ $Na_2V(PO_4)_2$ (NVP). The traces with high intensity at 17.99° indicates the tetragonal phase of $Na_2V(PO_4)_2$ in $NaVOPO_4$ and it is concreted by Raman analysis by peak shifting from 884 to 866 cm^{-1}. The character in $Na_2V(PO_4)_2$ influences the Na ion intercalation process and yields the specific capacity in a three-electrode system is 0.83mAh/g at the scan rate of 10mV/s.

(Received August 27, 2023; Accepted November 24, 2023)

Keywords: Cathode material, Na ion battery, $NaVOPO_4$/ $Na_2V(PO_4)_2$, Electrochemical properties

1. Introduction

Vanadyl phosphates are the most energizing cathode material for studying the interaction between alkaline ion chemistry and its host structure, resulting in Li-ion's very high stability, voltage profile, and electrochemical chemistry. However, the exploration of this type of Na has resulted in lower stability and poor electrochemical performance. Layered oxide material with open interstitials reduces the volumetric and gravimetric energy density of the material, but $(PO_4)^-$ polyanions create separated redox centres, giving rise to mixed valance electronic conductivity [1-5]. Furthermore, the inductive effect of the polyanionic compound associated with multiple redox couples is one of the elegant materials to achieve high capacity. $VOPO_4$ uses the V^{3+}/V^{4+}, V^{4+}/V^{5+} redox couples and crystallises in seven distinct polymorphs [6-7]. When Na ion is inserted into the ε – VOPO4 matrix, the monoclinic α –$NaVOPO_4$ will be formed, insertion of Na in α_1–$VOPO_4$ crystallizes the $NaVOPO_4$ into α_1 tetragonal, Na ion in β–$VOPO_4$ form β orthorhombic structure [9,10]. The Na ion insertion into this, change the V – O bond length and O(1) and O (2) sites. So the vanadium reduction state 5^+ in $VOPO_4$ is decreased to 4^+. Then there are four nearest V atoms surrounding the Na ion and it reduced the bond length of Na(1) and V(1). Due to that strong affinity arises between these two restricting the intercalation of Na (1). Song et al synthesized monoclinic α –$NaVOPO_4$ by sol-gel with the method with the discharge capacity of 20mAg/h at the rate of 0.05C [11]. If one more Na ion is inserted into $NaVOPO_4$, the Na – V distance is increased due to coulombic repulsion hence forth density of intercalated Na ions enriched. Moreover, its theoretical capacity also rises to 248mAg/h as well as changes the V reduction states. The E hull is extremely different for Na_2VOPO_4 and enriches the durability during the intercalation process of Na ion [12]. In this work, we attempt to feed one more Na ion experimentally into the $NaVOPO_4$ matrix to enhance the capacity and stability of $NaVOPO_4$. Sol gel-assisted hydrothermal method, pure sol-gel, and solid-state reaction methods are used in conjunction with high-temperature sintering. The samples synthesised by these three procedures are referred to as HT, SG, and SS, respectively. However, a reductive agent carbon, is essential to

* Corresponding author: nskdnp@gmail.com
https://doi.org/10.15251/JOR.2023.196.673

the process of incorporating more Na ions in $NaVOPO_4$, because it changes the O environment in the vicinity of the Na and V atoms, introducing an additional Na ion into the matrix. In the case of the pure solgel approach, 90% of citric acid is used as a gelating agent in the initial process, hence its residue causes only a few planes of $Na_2V(PO_4)_2$, whereas, in the solid state, citric acid is not added as a precursor resulting in only one Na ion inserted and it yields monoclinic phase. In the sol-gel-assisted hydrothermal method, the presence of reductive agent carbon at high temperatures causes $NaVOPO_4/Na_2V(PO_4)_2$ (NVP). The synthesized $NaVOPO_4/Na_2V(PO_4)_2$ (NVP) is having an electrochemical performance with a specific capacity of 0.2858 mAh/g at a scan rate of 100 mV/s.

2. Experimental techniques

There are three alternative ways to create the NVP cathode material: sol-gel-assisted hydrothermal, pure solgel, and solid state reactions.

2.1. Sol-gel-assisted hydrothermal method

The compounds namely Na_2CO_3 (Sigma and > 99.5%), NH_4VO_3 (Merck and > 99.0%), $NH_4H_2PO_4$, (Merck and 99.999%), and $C_6H_8O_7.H_2O$ (Merck and > 99.0%) are used as starting materials in this report. The 30ml of distilled water is combined with the $C_6H_8O_7.H_2O$, and the mixture is agitated for up to 30 minutes. The remaining precursors are added to the aforementioned solution and stirred for up to five hours. After that, the solution is transferred into an autoclave and heated to 180°C for 24 hours. The resultant gel-like solution is stirred and dried at 80oC. Then the powder is subjected to pre- and post-sintering at 350 and 550oC, respectively. The final product, which is olive green in colour is stored in an airtight container

2.2. Sol gel method

NVP samples are generated by the sol-gel technique. After the appropriate molecular weight of citric acid has been dissolved in 50ml of deionized water, the relevant stoichiometric amounts of Na_2CO_3, NH_4VO_3, and $NH_4H_2PO_4$ are added to the solution. The gel subsequently forms after few hours of stirring the solution at 80°C. After that, the gel is dried for 12 hours at 100 °C. Finally, the olive green powder can be obtained through pre- and post-sintering processes at 350°C and 550°C for 4 hours each in an air atmosphere.

2.3. Solid state reaction

Precursors with the appropriate mole ratio are ground separately for up to seven hours in a mortar and pestle. After that, the three compounds are mixed together and ground for four hours in a mortar. The pre- and post-sintering processes are applied to the mixed powder for 4 hours each at 350 and 450oC. Final olive green coloured product stored in a vials.

The crystal structure of the prepared materials are examined with X-ray diffraction (3^{rd} generation Empryrean, Malvern Panalytical multipurpose diffractometer) in the 2θ range of 5º- 90º . Furthermore, the crystal structure has been emphasized with Raman spectroscopy (WiTec alpha300, Germany) in the spectral range 50 – 4000 cm^{-1} with a 532nm excitation laser source. The surface morphology and energy dispersive spectra of the samples are observed with a field emission scanning electron microscope with EDS (energy dispersive spectrometer) TESCAN MIRA3 and ZEISS. IR vibrational spectra are obtained in the frequency range 400– 4000 cm^{-1}using Shimadzu FTIR spectrometer. Thermo Gravimetric Analyser (TG/DTA - EXSTAR/6300) is used to perform thermal analysis on the synthesized samples with a temperature range of 30ºC to 1000ºC under air at a heating rate of 20°C min^{-1}.

2.4. Electrochemical characterization

The electrodes are fabricated by mixing 85 wt. % of the active material (HT) with 10 wt. % of Carbon black and 5 wt. % binder (Polyvinylidene fluoride, PVdF), N- Methyl 2 – pyrrolidone (NMP) as a solvent. The mixture is coated on a copper plate which acts as a current

collector and dried at 80 °C for 12 h in a Hot air oven to ensure complete evaporation of the solvent NMP. The electrochemical performance of the pure and doped samples is studied using an electrochemical workstation Biologic SP- 150 in the three-electrode system with prepared NVP, Ag doped NVP samples as working electrode, Ag/AgCl as a reference electrode and Platinum electrode as counter electrode and 1M NaOH solution as an electrolyte solution.

3. Result and discussion

3.1. XRD

The XRD pattern of HT, SG, SS samples are shown in Fig.1.The peaks of the tetragonal and monoclinic phases are more apparent in the HT samples. The O (2 & 3) sites are occupied by the second Na(2) ion. As a result, it modifies the bond length V – O and forms the $[VO]_5$ pyramids. However, the initial Na ion in the Na (1) position increases the number of coordination with O to seven [13]. This has caused $[VO]_6$ to grow and develop the monoclinic residue at 18.32° in the plane of (110). At high temperatures, the reductive agent carbon reduces the V^{4+}/ V^{5+} to V^{3+}/ V^{4+}. As a result, the corner-sharing O fluctuates between $[VO]_5$ and $[VO]_6$ pyramids, which causes the monoclinic and tetragonal phases to grow in the synthesised material [14]. Citric acid is not added as a precursor in the solid-state reaction; hence, no by-product carbon is produced throughout the reaction. Additionally, only the strong peaks with high-intensity planes (110), (111), and (-212) are apparent, making the monoclinic phase the only dominant phase. The tetragonal phases at (201), and (310) are injected between monoclinic phases using the pure sol-gel approach since carbon is present at the high temperature. However, well-defined peaks do not form as they do when using the sol-gel assisted hydrothermal process due to poor crystalline nature. SG and SS samples are not showing the good crystallinity hence the solgel assisted hydrothermal process is the most effective way to introduce the second Na ion into the $NaVOPO_4$ matrix.

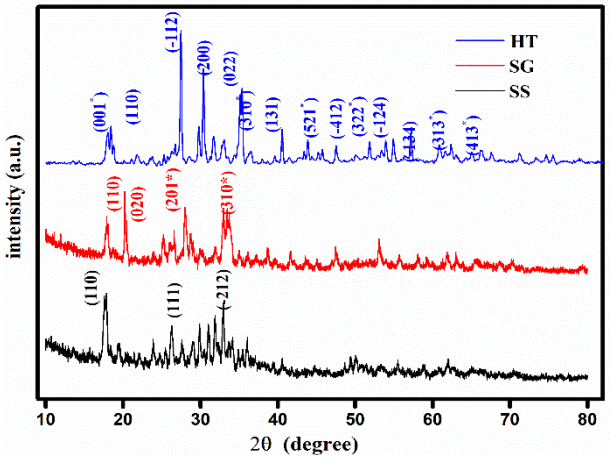

Fig. 1. XRD pattern of synthesised materials via a) sol-gel assisted hydrothermal, b) pure sol-gel, c) solid-state reaction.

3.2. FTIR analysis

The vibrational modes of synthesised samples such as HT,SG,SS are shown in Fig.2. Na – O and $\nu_2(PO)_4$ modes of vibration are seen in all three samples at 499cm^{-1}. The typical vanadyl bond ν(V═O) vibrations are visible at 829cm^{-1} in the SS sample and are more pronounced at 877cm^{-1} in the HT sample [15]. Conversely, the intensity in the SG sample is relatively low. As a result of the corner-sharing of O swings between $[VO]_5$ and $[VO]_6$, $\nu_1(PO)_4$'s substantial splitting at 959cm^{-1} is not observable, and v3(PO)4's symmetric stretching vibration shifts to a higher wave number at 1012cm^{-1} in the HT sample. When compared to the sample HT, the SG sample's Na(2)

site in O is severely constrained, which results in weak vibrations of $\nu_1(PO)_4$ and $\nu_3(PO)_4$ observable at 959cm^{-1} and 1089, 1159cm^{-1} respectively[16,17]. However, in the sample SS, the vibrations at and 1089, 1159cm^{-1} are very apparent which is due to the phase pure monoclinic. The ν_3 vibration band of PO_4 groups at 1221cm^{-1} is seen in the HT sample but in the case of SG and SS, it is blue-shifted to 1259cm^{-1}. Due of the sample's moisturising properties, the O – H vibrations are more pronounced in SG and SS samples. However, the O – H vibrations in the sample HT decreased its intensity. Vibrational modes are more prominent in the HT sample only and their frequencies are tabulated in Table 1.

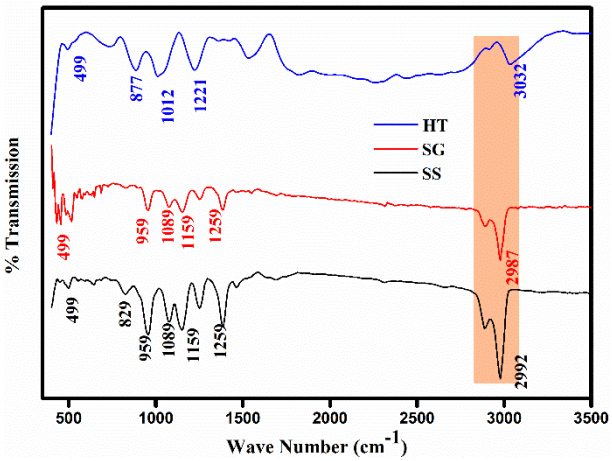

Fig. 2. Vibrational modes of synthesised materials via a) sol-gel assisted hydrothermal, b) pure sol-gel, c) solid-state reaction.

Table 1. Vibrational frequency assignments of SS, SG and HT samples.

Assignment	SS (Wave number cm $^{-1}$)	SG (Wave number cm $^{-1}$)	HT (Wave number cm $^{-1}$)
The bending vibration of Na – O and PO_4	499	499	499
Asymmetric stretching vibration (ν_1) of the PO_4 tetrahedral	959	959	NA
symmetric ν_3 of PO_4 tetrahedral	1089 ,1159,1259	1089, 1159,1259	1012,1221
V═O bond characteristic of the vanadyl compound	829	Nil	887
O – H	2992 (more prominent)	2987	3032 (poor intensity)

3.3. Raman analysis

Raman spectra of the synthesized samples are displayed in Fig. 3. The broad vibration peak at 286cm^{-1} of Na – O and lattice mode vibrations are shown in SS sample and it is less prominent in SG due to the enhancement of VO_5 pyramids. The Na(2) site modifies the V – O and Na(1) coordination's bond length, and as a result, the Na – O and lattice mode vibrations exhibit poor intensity in the HT sample [18]. The vibration of $\nu_2[PO]_4$ at 314, 386cm^{-1} is introduced by the lower site symmetry of C_{4v} in HT [15], whereas it is absent in the samples of SS and SG. The characteristic ν(V═O) vibration has a sharp intensity in the HT sample at 884cm^{-1} and it is blue-shifted due to the coordination alterations of Na (1) ions [13]. Conversely, the sample SS and SG

redshift the characteristic ν(V═O) vibration to 938cm^{-1}. This is due to the poor crystalline nature of the synthesised samples.

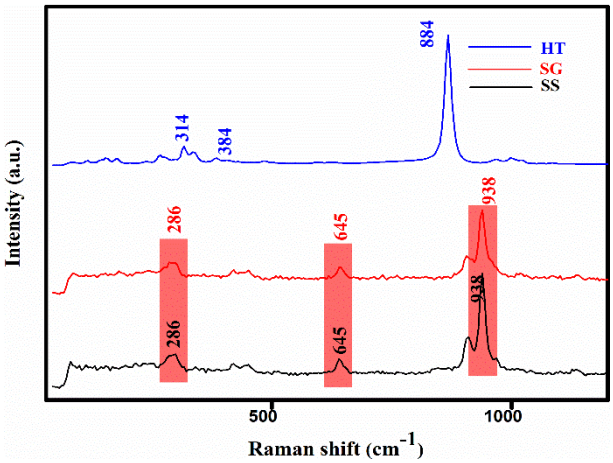

Fig. 3. Raman spectra of synthesised materials via a) sol-gel assisted hydrothermal, b) pure sol-gel, c) solid-state reaction.

3.4. Morphological analysis

The morphology of the HT sample are depicted in Fig. 4(a and b). Due to the HT sample's crystallinity, which is subject to the FESEM investigation. Particles of a rectangular shape are dispersed throughout the sample, according to the morphological investigation. Tetragonal phases are developed in plane (001), moreover, it allows the particle growth along the length of this rectangular particle.

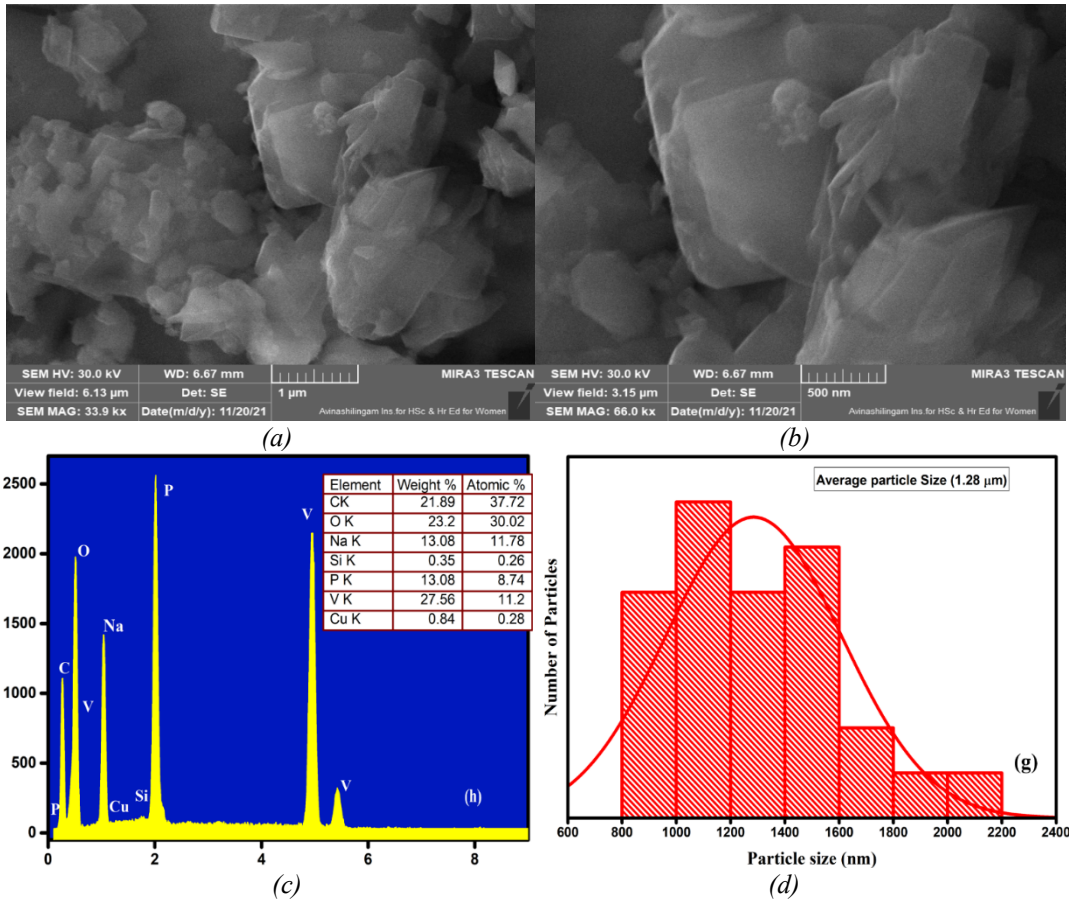

Fig. 4. (a and b) FESEM (c and d) EDS spectra and particle size distribution of HT sample.

Figure 5c displays the EDS spectra of NVP. The presence of carbon and Cu peak has emerged in the spectrum due to the carbon tape used for mounting the sample and Cu due to residues present at the sample holder. The weight percentage of EDS results is in good agreement with theoretical values of pure NVP (Na% = 13.12%, V% = 27.75%, P % = 13.18%, and O% = 22.74%). The average particle size is 1.28 µm which is calculated by using Image J software and is shown in Fig. 5d.

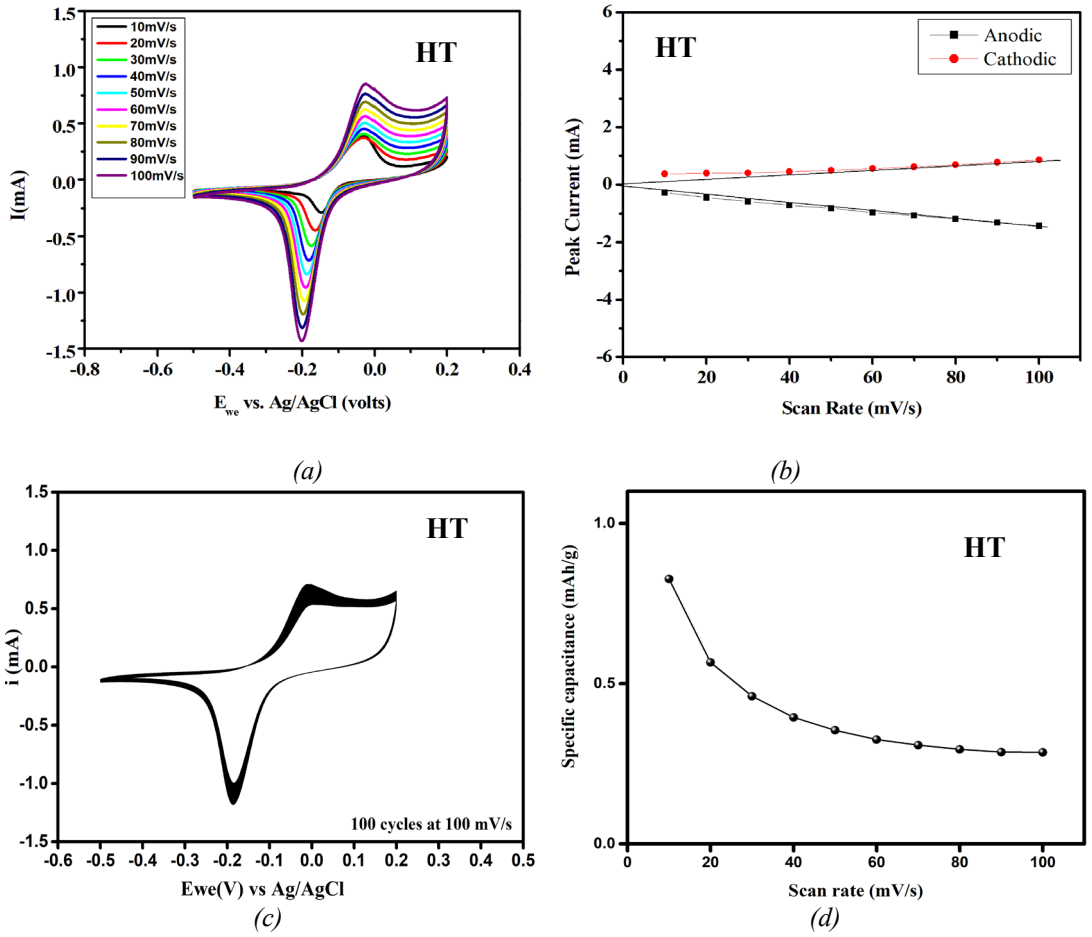

Fig. 5. (a) CV with different scan rates (b) linear plot (c) cyclic stability at the scan rate of 100mV/s (d) scan rate Vs specific capacity.

3.6. Electrochemical analysis

Since the SS and SG samples' weak crystallinity makes them unsuitable for electrochemical examination, the sample HT is submitted to the electrochemical investigation. The CV with different scan rates of HT samples are shown in Fig 5a. The potential separation of 10mV/s and 100mV/s is quite small hence the process is reversible. At 100 mV/s, the outer active surface of NVP is used to store the Na ions with a time constraint, whereas at low scan rates, the whole surface area is utilized which is achieved by ion insertion associated with capacitance behaviour [19,20]. The E_{we} of the anode peak has increased and the cathode peak E_{we} has decreased with an increase in scan rate, which intimates greater polarization at higher scan rates. The specific capacitance calculated at 100 mV/s scan rate of NVP pure is 0.2858 mAh/g. The linear plot of NVP is shown in Fig. 5b and it shows quasi-reversibility due to the varied slopes between anodic and cathodic reactions which is more prominent in the HT sample. The linear plot curves of HT samples are not passing through zero which implies the prevalence of faradic anode

peak current at very low scan rates up to 40mV/s and it is shown in Fig. 5c. These deviations could be due to the adsorption of species on the electrodes and the slow kinetics observed at lower scan rates. The VO_5 pyramids are growing conspicuously and the tetragonal crystalline phase formed in HT samples has enhanced as a result of the tetragonal phases in the monoclinic phase rearranging the oxygen-sharing arrangement between the phases and it exhibits stable CV curves after 100 cycles in Fig. 5d, proving that samples are electrochemically stable.

4. Conclusion

We synthesized the cathode material by sol-gel-assisted hydrothermal, pure sol-gel, and solid state reaction methods. The introduction of one more Na atom into the $NaVOPO_4$ material is only via facile sol-gel-assisted hydrothermal method which causes Na_2VOPO_4 in the $NaVOPO_4$ matrix. The complete evolution of Na_2VOPO_4 is not processed due to the O site symmetry alterations and it accompanies the VO_6/VO_5 chains. The high-intensity peak initiates the Na_2VOPO_4 tetragonal phase however, the site symmetry of O in the presence of a reducing agent from carbon makes the Na coordination with VO_6/VO_5 chains, hence monoclinic phase emerged at 27.35^o and it dominates the tetragonal phase. This is well agreed by Raman shift of V═O characteristic bond, Na – O alterations in the FTIR spectrum. The electrochemical performance of HT is analysed by a three-electrode system and its specific capacity is 0.83mAh/g at 10mV/s.

References

[1] S. W. Kim, D. H. Seo, X. H. Ma, G. Ceder, K. Kang, Adv. Energy Mater. 2, 710-721 (2012); https://doi.org/10.1002/aenm.201200026

[2] H. Kim, R. A. Shakoor, C. Park, S. Y. Lim, J.-S. Kim, Y. N. Jo, W. Cho, K. Miyasaka, R. Kahraman, Y. Jung, J. W. Choi, Adv. Funct. Mater. 23, 1147-1155 (2013); https://doi.org/10.1002/adfm.201201589

[3] Y. Zhu, Y. Xu, Y. Liu, C. Luo, C. Wang, Nanoscale.5, 780-787 (2013); https://doi.org/10.1039/C2NR32758A

[4] P. Barpanda, J.-N. l. Chotard, N. Recham, C. Delacourt, M. Ati, L. Dupont, M. Armand, J.-M. Tarascon, Inorg. Chem. 49, 7401-7413 (2010); https://doi.org/10.1021/ic100583f

[5] N. Ben Mansoura , G. Khouqeerb , N. Abdel Allb,c , J. El Ghoul, Journal of Ovonic Research 18, (2022), 57 – 65; https://doi.org/10.15251/JOR.2022.181.57.

[6] C. Ling, R. Zhang, F. Mizuno, J. Mater. Chem. A. 2, 12330-12339 (2014); https://doi.org/10.1039/C4TA01708K

[7] J. Song, M. Xu, L. Wang, J. B. Goodenough, Chem. Commun. 49, 5280- 5282(2013); https://doi.org/10.1039/c3cc42172d

[8] M. Hellenbrandt, Crystallogr. Rev. 10, 17-22 (2014); https://doi.org/10.1080/08893110410001664882

[9] G. He, A. Huq, W. H. Kan, A. Manthiram, J. Chem. Mater. 28, 1503-1512 (2016); https://doi.org/10.1021/acs.chemmater.5b04992

[10] R. Gopal, C. Calvo, J. Solid State Chem.5, 432-435 (1972); https://doi.org/10.1016/0022-4596(72)90089-8

[11] S. Li, Y. Dong, X. Lin, X. Xu, H. Liang, L. Mai, Adv. Mater. 26 (2014) 3545-3553; https://doi.org/10.1002/adma.201305522

[12] Huu Du Luong, Thi Dung Pham, Yoshitada Morikawa, Yoji Shibutania, Van AnDinh, J. Name. 00, 1-3 (2013).

[13] El abadila Iffer, Mohammed Belaiche, Chouaib Ahmani Ferdi, Moustapha Elansary, Abdul Khader Sunar,Yanxia Wang, Yuliang Cao, Int J Energy Res. 45, 1-17 (2020); https://doi.org/10.1002/er.5835

[14] Y C Lin, Marc F. V. Hidalgo, Iek-Heng Chu, NA. Chernova, M. S Whittingham, Shyue Ping

Ong, J. Mater. Chem.A. 5 17421-17431 (2107); https://doi.org/10.1039/C7TA04558A
[15] Enrique J. Baran and Marta B. Vassallo, Kwang-Hwa Lii, J Raman Spec. 25, 199-202 (1994); https://doi.org/10.1002/jrs.1250250302
[16] G. Janauer, A. Dobley, J. Guo, P. Zavalij, M. Whittingham, Chem. Mater. 8, 2096-2101 (1996); https://doi.org/10.1021/cm960111q
[17] Kang Hua, Xiujuan Lia, Rui Bao, Dong Fanga, Ming Jiang, Jianhong Yi, Zhiping Luo, Yongchun Shu, Benshuang Sun, Solid State Ionics 325, 133- 140 (2018); https://doi.org/10.1016/j.ssi.2018.08.002
[18] Sarah J. Greaves, William P. Griffith, Journal Of Raman Spectroscopy, 19, 503-507 (1988); https://doi.org/10.1002/jrs.1250190803
[19] G. Z. Fang, Z. X. Wu, J. Zhou, C. Y. Zhu, X. X. Cao, T. Q. Lin, Y. M. Chen, C. Wang, A. Q. Pan, S. Q. Liang, Adv. Energy Mater. 8 1703155 (2018); https://doi.org/10.1002/aenm.201870092
[20] R. N. Reddy, R. G. Reddy, J. Power Sources 156, 700 - 704 (2006); https://doi.org/10.1016/j.jpowsour.2005.05.071